ISSN 0020-1685, Inorganic Materials, 2015, Vol. 51, No. 15, pp. 1508–1514. © Pleiades Publishing, Ltd., 2015.
Original Russian Text © O.V. Kudryakov, V.N. Varavka, 2014, published in Zavodskaya Laboratoriya. Diagnostika Materialov, 2014, Vol. 80, No. 11, pp. 48–53.

MATERIAL MECHANICS: STRENGTH, LIFETIME, AND SAFETY

Integrated Indentation Tests of Metal-Ceramic Nanocomposite Coatings

O. V. Kudryakov* and V. N. Varavka

Don State Technical University, Rostov-on-Don, Russia

**@e-mail: kudryakov@mail.ru*

Received February 18, 2014

Abstract—The results of a study of the strength and erosive properties of ion plasma layered coatings of various metal and ceramic (nitride) systems are described. The total thickness of the coating is a few microns, while the thickness of each of the layers does not exceed two or three tens of nanometers. The use of different indentation schemes provides a set of physicomechanical properties responsible for the coating strength. The properties are subjected to multiparametric optimization to obtain a satisfactory correlation with the data of bench erosion tests of the coatings. It is found that the erosion resistance of nanocomposite coatings, which is commonly determined in complex bench or full-scale tests, can be reliably diagnosed from the set of the physicomechanical properties of the coatings measured in the laboratory.

Keywords: wear-resistant coating, structure and properties of coatings, nanocomposite materials, indentation, micro- and nanohardness, sclerometry, erosion resistance

DOI: 10.1134/S0020168515150108

One of the most common applied problems of diagnostics of materials is the reliable prediction of hardly identifiable performance properties of a material according to other characteristics of this material that can be measured using simple and standardized techniques and tests. This problem becomes even more complicated if the object of examination, measurement, and operation is a coating with micron thickness. This is true of, for example, the study of materials and coatings that are resistant to droplet impingement erosion. This kind of erosion is undergone by the blade system of powerful steam turbines: the cooling steam becomes wet and the resulting drip condensate becomes a source of erosion of the turbine blades rotating at high speed. The resistance of the material of the blades to droplet impingement erosion can be measured only in cost-intensive long-term bench or full-scale tests. In this context, the aim of this study was to examine the strength and erosion resistance of nanocomposite coatings, determine the correlation between these properties, and, as a consequence, explore the possibility of predicting the erosion resistance of coatings according to the strength properties of the coatings.

The following 2D metal-ceramic nanocomposite coatings were selected for the study: Ti/C, Ti/Mo, TiN/MoN, Ti/AlSi, TiN/AlSiN, Ti/Zr(Nb), and TiN/Zr(Nb)N. The coatings were deposited using an ion plasma spraying setup equipped with a magnetron evaporation system. The coating deposition modes were selected so as to provide the formation of dense (defect-free, nonporous) nanolayers with a nanocrystalline structure and compressive stresses in the coating. Samples of steel 20Kh13 with a sorbitol structure (quenching + high-temperature tempering) of the KP 50–60 strength class with a surface roughness of R_z = 0.08 μm were used as a substrate. The chemical composition of the coating was determined by the composition of the magnetron target (electrode) and the composition of the gas in the vacuum chamber of the setup. The coating composition was additionally controlled using an X-Max EDAX energy-dispersive electron probe microanalyzer (Oxford Instruments); the amorphous components of the coatings were identified by X-ray diffraction analysis on a DRON-7 diffractometer using Fe$K\alpha$ radiation.

The structure of the nanocomposite coatings was studied using a Mira Tescan 3 LMU scanning electron microscope (SEM) operating in a wide range of magnifications including the nanolevel of the structure. The microstructures of some types of the studied coatings are shown in Fig. 1. The typical structure of a 2D nanocomposite coating is shown in Fig. 1a. This structure was found in the Ti/C, Ti/Zr(Nb), Ti/Mo, and TiN/MoN coatings. A characteristic feature of these coatings is the presence of dense defect-free nanolayers exhibiting no signs of a grain structure. Figure 1b shows an example of an amorphized structure of the coating; the formation of this structure is attributed to the presence of silicon in the system. Figure 1c shows the effect of the substrate topography on the coating quality: the initial surface roughness of the base metal

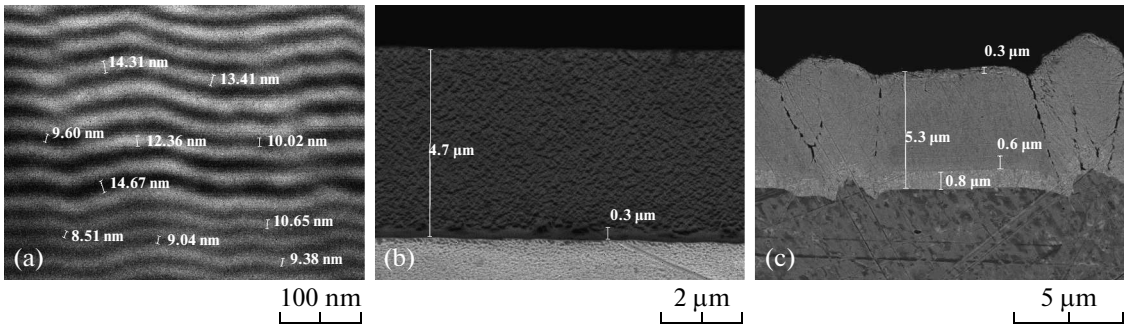

Fig. 1. Cross-sectional microstructure of the nanocomposite coatings (SEM images): (a) the nanolayers of the TiN/MoN coating, (b) the amorphized Ti/AlSi coating, and (c) the TiN/Zr(Nb)N coating.

(steel 20Kh13) is responsible for the occurrence of growth defects, discontinuities, and stresses in the coating, which adversely affect both the strength and erosion resistance of the coating despite the presence of nanolayers in it.[1]

Many studies have shown that indentation is the most effective method for predicting the physicomechanical properties of the surface layers of metals, including the coatings [1–3]. In this study, the physicomechanical properties of coatings were examined by indentation and scratching at different scale levels under the action of varying indentation load. Vickers microhardness (*HV*) was determined in accordance with GOST (State Standard) R ISO 6507-1–2007 using a DuraScan 20 hardness tester with the automatic (electro-optical) measurement of the indent. The nanohardness was determined using a NanoScan-3D scanning nanohardness tester (Technological Institute for Superhard and Novel Carbon Materials, Troitsk, Russia) under continuous instrumental indentation.

To provide measurements in the nanometer range, loads and indentation rates were selected according to the recommendations of GOST 8.748–2011. The summarized results of measurements of the geometrical parameters of the coatings obtained by SEM metallography and the tensile properties determined by the indentation method are shown in Table 1. Despite the use of a load of 10 g, which is the minimum possible load for the DuraScan 20 instrument, the determined microhardness of the coatings of some systems was lower than the expected value. This fact is indicative of the effect of a "soft" substrate (steel 20Kh13) and characterizes microhardness as a less reliable method for the diagnostics of these coatings than nanohardness.

The adhesion and scratch resistance of the coatings, the coefficient of friction between the different regions of the material, and other physicomechanical properties were determined in sclerometric tests conducted using a multimodule scratch tester (CSM Instruments, Switzerland). Using the CSM scratch tester, the most informative data set with a wide range of strength parameters was derived. The nanocomposite coatings of all the studied systems were tested in the loading mode with a variable normal load linearly increasing from 0.03 to 30 N. The mode provided the indenter penetration through the entire thickness of the coating into the base metal at a scratching rate of 5 mm/min and a rate of rise of load of 30 N/min. The test time was 1 min; the scratch length was 5 mm. The scratch-test conditions are shown in Fig. 2a; one of the test results (for the TiN/AlSiN coating) is represented in Figs. 2b–2d.

The technique for determining the strength characteristics of the coating in the scratch tests was as follows. During loading, the instrument recorded plots of variation in the normal force, the coefficient and force of friction (Fig. 2b), the penetration depth of the indenter during the application of load, and the residual depth after the removal of load (Fig. 2c), as well as the signal of the acoustic emission sensor (Fig. 2d), whose reflections characterize the occurrence of cracks. The two axes of abscissas in Figs. 2b–2d are the scales of variation in load (in newtons) and crack length (in millimeters). The micrographs of the scratch (Figs. 2b–2d show the optical image of the scratch above the plots) are used to determine the time of crack nucleation in the coating ((Lc1) not shown in Fig. 2) and the incipient (Lc2) and complete delamination of the coating (Lc3). In Figs. 2b–2d, the left-hand side of the scratch and the plots (to the left of Lc2) corresponds to the coating, while the right-hand side (to the right of Lc3) characterizes the base metal.

CSM scratch testers have a high-precision optical positioning system with a CCD camera that provides the examination of scratches at high magnifications.

[1] A growth defect of a coating is understood as the violation of the homogeneity of a coating during the layer-by-layer deposition (growth) of the coating. For example, at a high roughness of the substrate, the layer-by-layer growth is violated because the number of layers on the protrusions and depressions of the relief is not the same. This feature leads to the formation of internal interfaces (boundaries) and fragmentation of the coating structure.

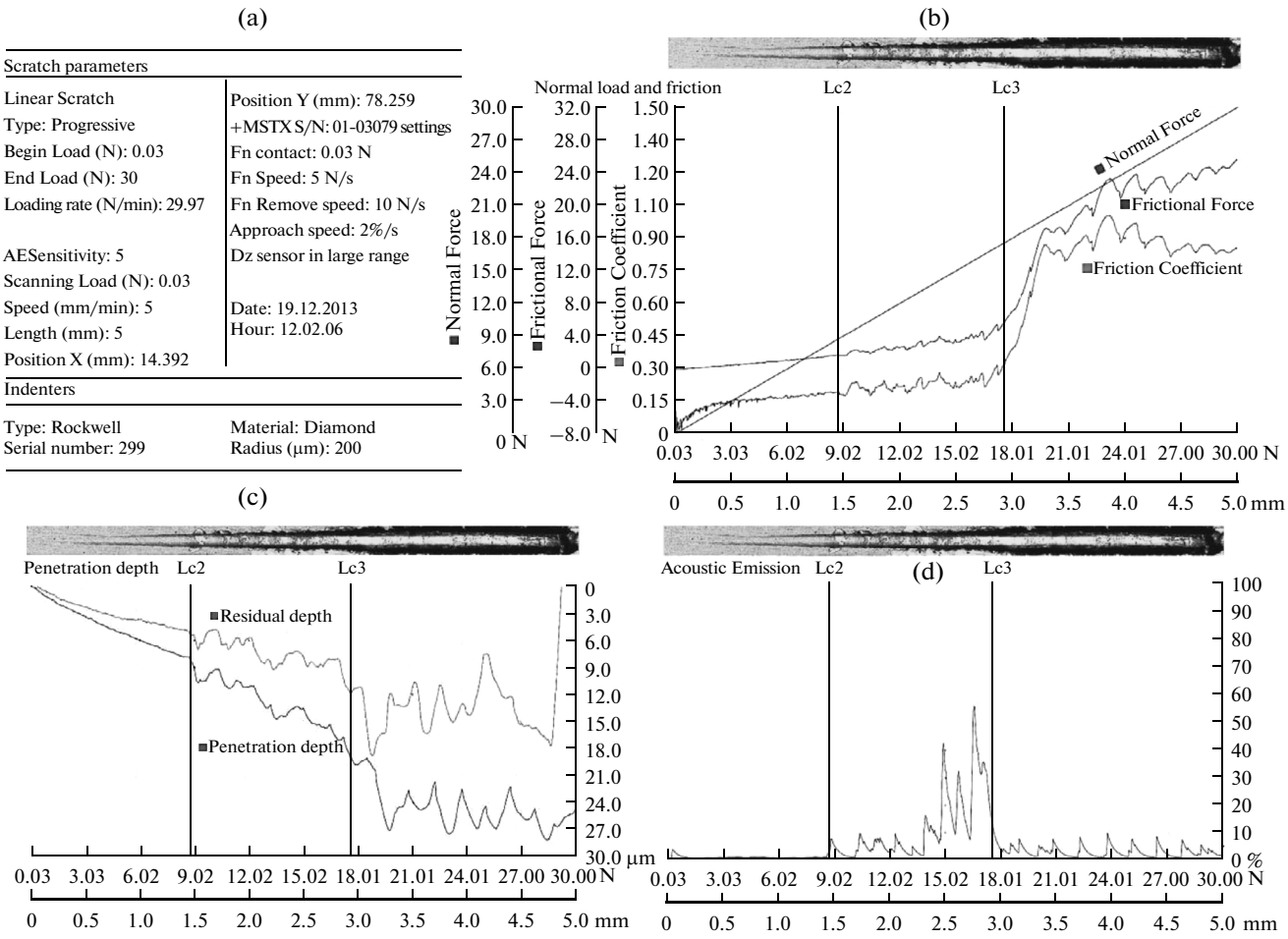

Fig. 2. (a) Conditions and (b–d) results of the scratch test of the nanocomposite coating of the TiN/AlSiN system: (b) sclerometric force diagrams, (c) the penetration depth of the indenter, and (d) acoustic emission.

However, in some cases, the identification of the morphological features of the sclerometric surface required a higher resolution. To this end, SEM images of the scratch were used; the images were studied after a similar superposition on the sclerometric diagrams. In particular, Fig. 3 shows the SEM image of the same scratch as in the upper portion of Figs. 2b–2d, to be more precise, a fragment of the scratch in the region of incipient delamination of the coating (Lc2). In the phase contrast mode (see the right-hand side of Fig. 3), it is clearly evident that, for the TiN/AlSiN coating, the instants of crack nucleation (Lc1) and incipient delamination (Lc2) coincide. This feature is characteristic of thin hard coatings with a relatively low adhesion to the base metal. The capillary nature of the cracks before the cleavage regions in Fig. 3 suggests that the coating has an amorphous structure.

The results of determination of the physicomechanical properties of the studied coatings using a multimodule CSM scratch tester are shown in Table 2. Here, the incipient delamination of the coating Lc2 is characterized by critical values of load P_1 and depth p_1, while the complete delamination Lc3 is described by critical values of P_2 and p_2, respectively.

Analysis of the data on the physicomechanical properties of the coatings derived by the different indentation methods (see Tables 1, 2) shows that none of the properties taken separately can unambiguously and reliably characterize the erosion resistance of the coatings. Therefore, a multiparametric optimization [4] of the strength properties of the coatings was conducted via integrating the ray diagrams. An example of this diagram for nanocomposite coatings of three systems is shown in Fig. 4. The relative values of nine physicomechanical properties listed in Tables 1 and 2 are plotted along the axes of the ray diagram: $HV_{0.01}$, nanohardness, E, P_1, p_1, f_1, N_1, P_2, and p_2. Since the number of parameters is quite large (nine) and no correlations of each of the parameters taken separately with erosion-resisting properties have been revealed, upon switching to the relative values of the parameters, their coefficients of significance (specific weights) were assumed to be equally probable. The maximum value of the property obtained during the tests (concerning the coatings of all the seven studied systems)

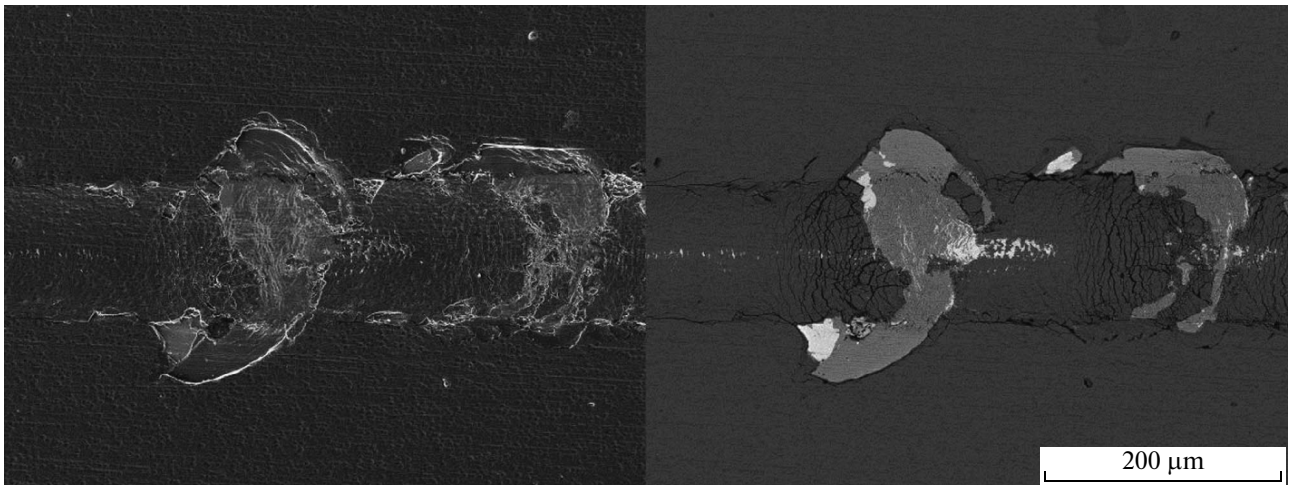

Fig. 3. Secondary electron (left) and backscattered electron (right) SEM images of the scratch of the TiN/AlSiN coating in the region of incipient delamination Lc2; the direction of travel of the indenter during scratching is from left to right.

was taken as a unit of each of the parameters except for the friction coefficient, for which the minimum value was taken as a relative unit. The area of the polygon in the diagram corresponding to each of the coatings was used as an integrated statistical relative estimation of the strength of the coatings; it was an optimization variable: the larger the area of the polygon, the greater the total strength of the coating. Area S of the polygon was calculated as the sum of the areas of its constituent n triangles:

$$S = \frac{1}{2}\left[a_1 a_n + \sum_{i=1}^{n-1}(a_i a_{i+1})\right]\sin\frac{2\pi}{n},$$

where n is the number of rays (properties) of the diagram and a_i is the relative value of the property of the coating in the diagram.

According to the multiparameter optimization results, the ion plasma nanocomposite coatings of the studied systems can be arranged in the following descending order with respect to strength (i.e., the set of nine physicomechanical properties): TiN/AlSiN, TiN/MoN, Ti/AlSi, Ti/C, Ti/Mo, Ti/Zr(Nb), TiN/Zr(Nb)N (Fig. 5). The fact that the TiN/Zr(Nb)N nitride system is the last in this series is attributed to the technological defects arising during formation—substrate topography, discontinuities, growth effects, and stresses—rather than to the nature and properties of the coating (see Fig. 1c).

Erosion tests were conducted using a unique special-purpose Eroziya-M test bench of the Moscow Power Engineering Institute (National Research University), which is employed for studying the resistance of materials and coatings to the effects of a high-veloc-

Table 1. Results on the indentation of samples with nanocomposite coatings

Type of coating	Microhardness (at load of 10 g)	Indentation depth $h_{0.01}$, μm	Coating thickness h, μm	Layer thickness, nm	Continuous indentation	
					nanohardness, GPa (at load of 1 mN)	elastic modulus E, GPa
Ti/AlSi	655–499 $HV_{0.01}$	0.76–0.87	4.7–9.3	Amorph	7.2(3.44*)–9.2**	148(76*)–232
Ti/Mo	776 $HV_{0.01}$	0.70	4.32	–	–	–
TiN/MoN	1974 $HV_{0.01}$	0.44	5.32	8.5–14.6	–	–
Ti/C	482 $HV_{0.01}$	0.89	2.2–2.9	10.1–12.5	7.1	179
Ti/Zr(Nb)	480 $HV_{0.01}$	0.89	5.4	10–12	7.36	141
TiN/Zr(Nb)N	270 $HV_{0.01}$	1.18	1.9–5.3	10.2–15.0	7.48	133
	–	–	7.1	25–30	3.95	180
TiN/AlSiN	948 $HV_{0.01}$	0.64	5.1	Amorph	8.01	166

* At a load of 10 mN.

** In the cross microsection.

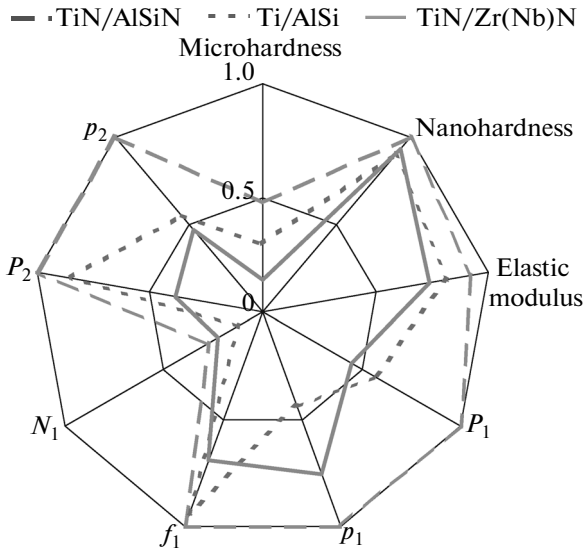

Fig. 4. Ray diagram of the physicomechanical properties of nanocomposite coatings of the TiN/AlSiN, Ti/AlSi, and TiN/Zr(Nb)N systems according to the data of Tables 1 and 2.

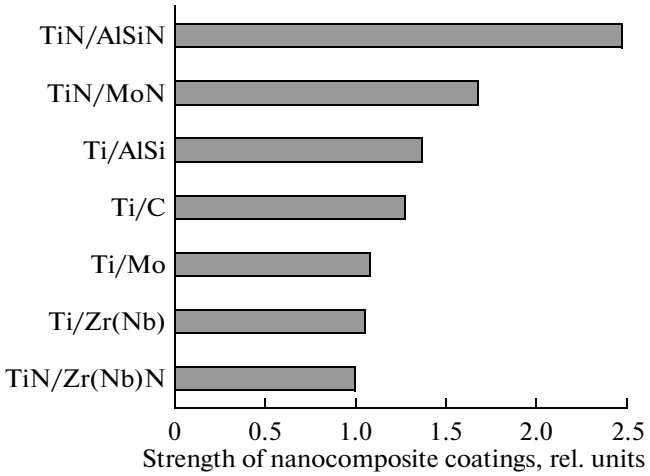

Fig. 5. Integrated strength of nanocomposite coatings of the different systems.

ity stream of liquid droplets [5–9]. The bench provides the simulation of different conditions of interaction of the liquid particles with the surface of materials, in particular, real conditions of the droplet impingement erosion of the blades of steam turbines. In this case, the variational parameters are the droplet diameter $d_{dr} = 20–1200$ μm and the collision velocity of liquid droplets with samples $C_{coll} = 200–600$ m/s. The test results are used to plot curves of the erosive wear of materials or coatings at fixed C_{coll} and d_{dr} values in the coordinates of test time t (min) or erodent (liquid) flow rate m (kg/m^2) versus wear, i.e., the loss of sample weight M (kg). In the general case, the droplet-impingement erosion wear occurs in three successive stages: incubation, during which $M = 0$; transition, which begins at time m_0 and where the development of wear occurs at a maximum average rate $\partial M/\partial m \rightarrow$ max; and an asymptotic stage of steady wear, during which $\partial M/\partial m \rightarrow$ min [3–6].

In [10, 11], it is shown that thin coatings perform a protective function only in the case of preservation of continuity. Therefore, comparison of the erosion resistance of the studied small-thickness nanocomposite coatings against each other and with other materials can be correctly conducted only according

Table 2. Results on the indentation of samples with nanocomposite coatings

Type of coating	Critical applied load P_1, N	Critical depth* p_1, μm	Average friction coefficient in coating f_1	Average friction coefficient in substrate f_2	Critical tangential force N_1, N	Complete coating cleavage force P_1, N	Critical depth* p_2, μm
Ti/AlSi	3.54–6.39	1.65–3.1	0.165–0.226	0.9	0.54–0.7	12.71–17.0	2.30–8.75
Ti/Mo	–	–	0.3–0.477	0.85	3.37	6.89	2.30
TiN/MoN	8.3	3.13	0.05–0.27	0.35–0.6	2.55	14.3	3.41
Ti/C	6.89	5.15	0.3–0.9	1.0	5.86	–	–
Ti/Zr(Nb)	6.23	–	0.246	0.9	1.51	13.09	–
TiN/Zr(Nb)N	1.36–6.31	1.64–6.53	0.149–0.38	0.8–1.1	0.23–2.39	4.58–9.07	4.44–6.48
TiN/AlSiN	8.83	5.48	0.183	0.9	1.62	17.54	11.71

* Determined from the plot of residual depth (see the "Residual depth" curve in Fig. 2c).

to the duration of incubation period m_0, during which the coating maintains its continuity. In addition, at the transition stage ($m > m_0$), there arises the problem of separating the contributions to the wear of the coating and the substrate. Therefore, the m_0 values of the materials and coatings obtained under identical conditions of bench tests were used as an antierosion index.

To compare the erosion resistance indices, steel 20Kh13 of the KP 50–60 strength class (a sorbitol structure after quenching and high-temperature tempering) is commonly taken as a base blade material (reference). The low m_0 value of the VT6 titanium alloy (see Fig. 6) is attributed to the fact that the samples were tested in an annealed state. The VT3-1 alloy, in common with VT6, is a two-phase titanium alloy ($\alpha + \beta$) of the martensite type. However, unlike VT6, the VT3-1 samples were tested in a precipitation-hardened state after quenching and aging.

The best results on erosion resistance are provided by the use of stellite (V3K), which shows a multiple decrease in the rate of droplet-impingement erosion wear compared to other materials [7]. The m_0 value of this alloy is the highest (see Fig. 6). However, in terms of technology, ion plasma coatings are more promising than stellite, which is used to protect the blades in the form of cast plates welded or soldered to the leading edges of a blade. This feature significantly complicates the manufacturing technology of blades and causes the occurrence of stress concentrators in the blades.

Among the studied nanocomposite coatings, the amorphized coatings of the Ti/AlSi and TiN/AlSiN systems are more resistant to the effects of droplet impingement than pure metal composites. Under these conditions, the nanocomposites of nitride systems exhibit the highest erosion resistance. The m_0 value of these composites is on the level of that of stellite. However, the most important result follows from comparison of the test data on the strength and erosion resistance of the ion plasma nanocomposite coatings: the sequence of arrangement of coatings in Figs. 5 and 6 is almost the same. An exception is provided by the coating of the TiN/Zr(Nb)N system, which had the lowest physicomechanical properties (see Fig. 5) and exhibited one of the highest erosion resistances (see Fig. 6). This feature is attributed to the fact that the samples with this coating selected for strength tests had the above technological defects (see Fig. 1c) in order to show the effect of the quality of the coating on the properties thereof. In the preparation of the samples for erosion tests, these technological defects were eliminated.

It can be concluded that there is a satisfactory correlation between the set of physicomechanical properties of the ion plasma nanocomposite coatings (nine characteristics obtained by the different indentation methods) and the erosion resistance of these coatings. This feature provides the possibility of a qualitative comparative prediction of the resistance of various coatings to droplet impingement erosion, which can be measured only in bench or full-scale tests, from the set of their physicomechanical properties measured in the laboratory.

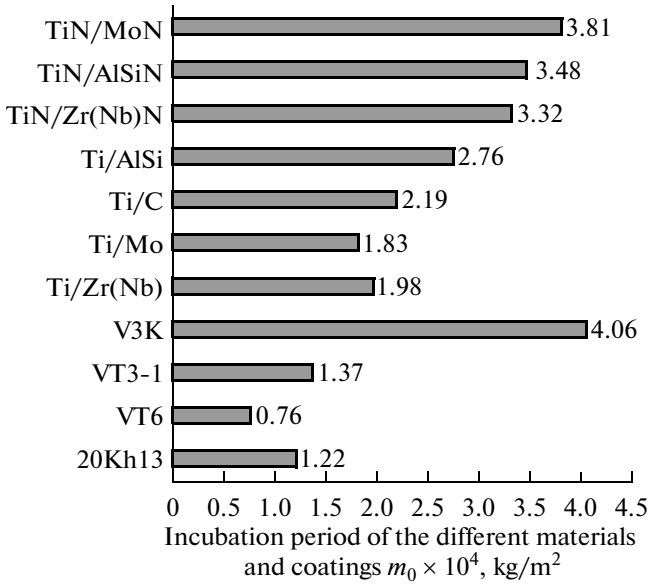

Fig. 6. Erosion resistance of typical blade materials and nanocomposite coatings of the different systems in the bench tests with the parameters of collision of C_{coll} = 250 m/s and d_{dr} = 800 μm.

Thus, the used set of nine physicomechanical properties that determine the strength of the coatings provides high coincidence with the results of erosion tests and can be recommended for the comparative characterization of the resistance of different coatings to droplet impingement erosion. In general, scratch tests provide more complete and accurate information on the erosion resistance of coatings than other types of indentation do. None of the nine measured properties of the coatings taken separately gave satisfactory agreement with the results of the erosion tests.

The nitride systems of nanocomposites exhibit the highest integrated strength (the set of nine studied physicomechanical characteristics) and antierosion properties of all the examined coatings. A positive effect on these properties is also exerted by the amorphization of the coatings.

The quality of ion plasma coatings, which is determined by the preparation of the substrate surface and the technological mode of coating deposition, has a significant impact on the properties of the coatings. The presence of growth defects, porosity, and stresses in the coating and irregularities and discontinuities on the substrate surface dramatically reduces both the integral estimate of strength and the erosion resistance of the coating regardless of the coating composition. Using the example of the TiN/Zr(Nb)N coating, it has been shown that all the used indentation techniques

are sensitive to these effects and nanoindentation exhibits the lowest sensitivity.

REFERENCES

1. Bulychev, S.I. and Alekhin, V.P., *Ispytanie materialov nepreryvnym vdavlivaniem indentora* (Testing of Materials by Continuous Indentation), Moscow: Mashinostroenie, 1990.
2. Matyunin, V.M., Strength methods in the diagnostics of materials: State-of-the-art, problems, and prospects, *Zavod. Lab., Diagn. Mater.*, 2004, vol. 70, no. 6, pp. 37–42.
3. Golovin, Yu.I., Nanoindentation as a tool for the integrated estimation of the physicomechanical properties of materials in submicrovolumes: A review, *Zavod. Lab., Diagn. Mater.*, 2009, vol. 75, no. 1, pp. 45–59.
4. Zedgenidze, I.G., *Planirovanie eksperimenta dlya issledovaniya mnogokomponentnykh system* (Experimental Design for Studying Multicomponent Systems), Moscow: Nauka, 1976.
5. Mednikov, A.F., Ryzhenkov, V.A., Seleznev, L.I., and Lebedeva, A.I., Studying the variation of parameters characterizing the material surface during the droplet erosion incubation period, *Therm. Eng.*, 2012, vol. 59, no. 5, pp. 414–420.
6. Seleznev, L.I. and Ryzhenkov, V.A., Erosion wear of constructional materials, *Tekhnol. Met.*, 2007, no. 3, pp. 19–24.
7. Ryzhenkov, V.A., Lebedeva, A.I., and Mednikov, A.F., Erosion wear of the blades of wet-steam turbine stages: Present state of the problem and methods for solving it, *Therm. Eng.*, 2011, vol. 58, no. 9, pp. 713–718.
8. Kudryakov, O.V. and Varavka, V.N., Mechanisms governing the formation of erosion wear of metallic materials during high-velocity droplet collisions: Part 1, *Materialoved.*, 2012, no. 5, pp. 36–43.
9. Kudryakov, O.V. and Varavka, V.N., Mechanisms governing the formation of erosion wear of metallic materials during high-velocity droplet collisions: Part 2, *Materialoved.*, 2012, no. 6, pp. 14–19.
10. Varavka, V.N. and Kudryakov, O.V., Specific features of degradation of metal alloys under conditions of continuous droplet impingement erosion, *Izv. Vyssh. Uchebn. Zaved., Tekh. Nauki*, 2012, no. 3, pp. 45–50.
11. Kudryakov, O.V. and Varavka, V.N., Monitoring of the initial stages of erosive wear of ion plasma coatings under droplet impingement conditions, *Uprochn. Tekhnol. Pokr.*, 2012, no. 10, pp. 40–47.

Translated by M. Timoshinina